J Mater Sci (2007) 42:7016–7030
DOI 10.1007/s10853-006-1117-1

Statistical model for characterizing random microstructure of inclusion–matrix composites

Ahmed Al-Ostaz · Anipindi Diwakar · Khalid I. Alzebdeh

Received: 9 April 2006 / Accepted: 10 October 2006 / Published online: 30 April 2007

Abstract The variation of arrangement of micro-structural entities (i.e. inclusions) influences local properties of composites. Thus, there is a need to classify and quantify different micro-structural arrangements. In other words, it is necessary to identify descriptors that characterize the spatial dispersion of inclusions in random composites. On the other hand, Delaunay triangulation associated with an arbitrary set of points in a plane is unique which makes it a good candidate for generating such descriptors. This paper presents a framework for establishing a methodology for characterizing microstructure morphology in random composites and correlating that to local stress field. More specifically, in this paper we address three main issues: correlating microstructure morphology to local stress fields, effect of clustering of inclusions on statistical descriptors identified in the paper, and effect of number of realizations of statistical volume elements (SVEs) on statistical descriptors.

A. Al-Ostaz (✉)
Department of Civil Engineering, University of Mississippi, University, MS 38677, USA
e-mail: Alostaz@olemiss.edu

A. Diwakar
SC Solutions, Inc., 1261 Oakmead Pkwy., Sunnyvale, CA 94085, USA

K. I. Alzebdeh
Department of Mechanical & Industrial Engineering, Sultan Qaboos University, Muscat, Sultanate of Oman

Introduction

There are many factors which influence stress fields in composite Materials: the mismatch in material constants, the shape and *geometric arrangement of inclusions*, the boundary conditions at inclusion–matrix interfaces, and proximity to the surface.

A fundamental problem in the evaluation of local stress fields is a single inclusion solution [1], which is applicable for dilute distribution of inclusions (i.e. composites with inclusions placed far apart from each other). When inclusions are closely spaced stress fields interact and solutions become very complex. In order to simplify this problem effective medium approaches, such as the Mori–Tanaka method, for example, based on a single inclusion solution, have been used in the analytical predictions of average stress fields [2–4]. Estimation of those averages presents a fundamental issue for different effective medium theories [5–7].

Numerical approaches usually involve assumptions that the arrangement of inclusions is periodic: square or hexagonal. However, the distribution of inclusions in composite materials is in general disordered. The periodic arrangement assumption may give good predictions for effective elastic and thermal constants, and average stresses and strains in composite materials, but they cannot capture local fields in composites with randomly arranged and interacting inclusions. The influence of random arrangement of inclusions on local fields and/or effective properties was studied by many researchers numerically [8–26], analytically [27] and experimentally [8, 28, 29].

The dispersion of inclusions and cracks in the transverse direction of composite materials has a very strong influence on the local stress fields and therefore, it affects the durability and fracture characteristics of the material. Therefore

it is necessary to re-define the unit cell concept so that it contains enough inclusions and cracks to be representative for the non-regular microstructure. Pijaudier-Cabot and Bazant [30] presented a method to calculate the stress field in a solid containing multiple inclusions and determined the stress intensity factors for a single crack situated among the inclusions. Another method for stress analysis in elastic solids with randomly distributed cracks was presented by Kachanov [31]. Both methods are based upon a superposition scheme and take into account the interaction between inclusions and cracks.

In this paper, we correlate random microstructure morphology of inclusion–matrix composites to local stress fields. Randomness in morphology is modeled using Voronoi tessellations and associated Delaunay triangulation networks. Effect of number of statistical volume elements (SVE) and effect of inclusions clustering on statistical descriptors of random composite is also presented.

Random composite

In order to study the random behavior of composite's microstructure; the randomness phenomenon has to be properly defined. Models of random media may be useful at two different levels: to provide a description of the heterogeneous structure, and to predict some macroscopic properties of materials. Randomness can be introduced into periodic networks in various ways. There are two basic probabilities; substitutional disorder and topological disorder. Substitutional disorder refers to variability in properties per vertex (or node) and topological disorder refers to a departure from the periodic topology. There is, also, a third case called the geometric disorder which refers to the variability in the geometry of a network's structure. Geometric disorder is the focus of this study.

By a random composite we refer to a set $B = \{B(\omega); \omega \in \Omega\}$ of deterministic media $B(\omega)$, where ω indicates one specimen (realization), and Ω is an underlying sample (probability) space [32]. All specimens $B(\omega)$ occupy the same domain in x_1x_2-plane, whereby a two-dimensional setting is employed for the clarity of presentation. Formally speaking Ω is equipped with a σ-algebra F and a probability distribution P.

For statically homogeneous media, it is reasonable and helpful to make the ergodic assumption which asserts that the volume average of stress of one specific σ (ω) over a given volume V equals the ensemble average of the random function $\sigma(\underline{x}, \omega)$ at any location $\underline{x}$ [32]. Mathematically, the ergodicity condition is stated as

$$\bar{\sigma} \equiv \frac{1}{V}\int_V \sigma(\underline{x}, \omega)\mathrm{d}x = \langle\sigma\rangle \equiv \int_\omega \sigma(\underline{x}, \omega)p(\omega)\mathrm{d}\omega \qquad (1)$$

where $\bar{\sigma}$ is the volume average stress over a fixed ω, while $\langle\sigma\rangle$ is the ensemble average over all specimens at fixed $\underline{x}$. By making such assumption, the statistics of the effective average stress σ can be determined from a single realization σ (ω).

In random matrix inclusion composites there are two aspects immediately noted:

- Spatial disorder: Formulation of random medium theory need to be adopted
- Periodicity on the scale of window L

Thus, these two aspects need to be considered whenever a simulation of *random* composite of an *infinite* medium is desired. Thus, in order to investigate a non-regular distribution of inclusions, the unit cell concept has to be defined in such a way so that it contains enough inclusions and cracks to be representative of the non-regular microstructure [33]. For the purpose of characterizing microstructure morphology of random composites, it is necessary to identify unique *descriptors* that in a best way characterize the spatial dispersion of inclusions. On the other hand, Delaunay triangulation associated with an arbitrary set of points in a given plane is unique which makes this method a good candidate for generating such descriptors. Related work was reported by [16, 18–25, 33–38].

Theory of Delaunay triangulation and voronoi cells

The theory of Delaunay triangulation is described in detail by Green and Sibson [39]. Generally, the Delaunay triangulation associated with an arbitrary set of points in the plane is unique. Thus this method represents a meaningful way of describing the local morphology of composite materials where the vertices of the Delaunay triangles represent the centers of the inclusions.

In order to generate Voronoi mosaic, first we generate random points $M_1, M_2 \ldots$ in plane according to a selected random process of density ρ points per unit area. Then, we subdivide the area into cells $C_1, C_2, \ldots$ by the rule: C_i cell contains all points in plane closer to M_i than to any other $M_j (j \neq i)$. M_i point is the center of C_i cell. In practice M_i represents the location of the original seed cell from which C_i grew. In this process, one assumes that:

- seeds of all cells start growing at the same instant,
- seeds grow at the same rate in all directions,
- seeds stop growing as they contact the neighboring ones.

Thus, a Voronoi tessellation of polygons is constructed by drawing the perpendicular bisectors of the line segments that connects a center with neighboring centers. This procedure assigns a unique area to each center and covers the plane of observation without overlapping. All points

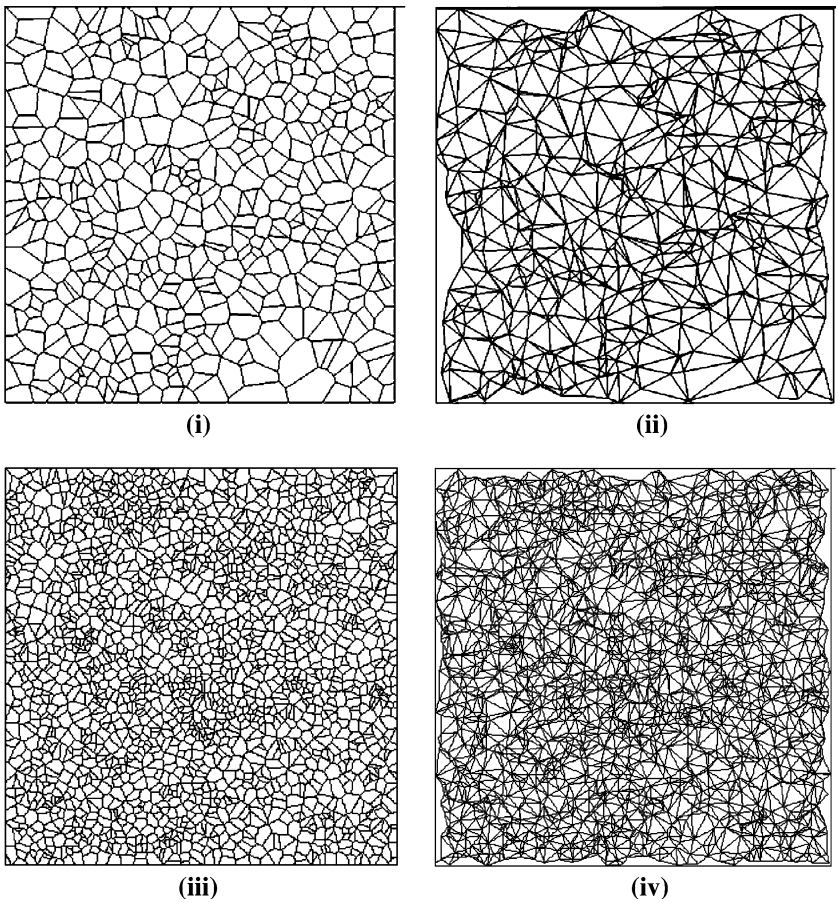

Fig. 1 (i) Voronoi polygons of 500 points (ii) Delaunay triangulation for 500 points, (iii) Voronoi polygons of 1,000 points and (iv) Delaunay triangulation for 1,000 point

enclosed in a polygon of the planar area are closer to its center than to any other polygon's center. It is then possible to identify all neighbors of a given center, and if necessary, to calculate statistics of neighbors distances and orientations. The dual Delaunay triangulation to the Voronoi tessellation is constructed by connecting all random points that share a polygon boundary. Typical Delaunay triangulation and Voronoi cells are shown in Fig. 1.

In general, the vertices of the Voronoi tessellation occur where three adjacent polygons meet. The three random points associated with each of these polygons form a Delaunay triangle. By definition, each vertex of a Voronoi tessellation is equidistant from each of the three data points forming the Delaunay triangle. Thus, each vertex of the Voronoi tessellation is uniquely associated with a Delaunay triangle and is located at its circumcenter. When the Delaunay triangulation is complete, this means that no data point may lie inside the circumcircle of any triangle.

In this paper four statistical *descriptors* are used: nearest neighbor distance; nearest neighbor angle with respect to horizontal axis X; cell size (Area of cell); and number of nearest neighbors (number of polygon sides). Figure 2 shows the schematic of the statistical descriptors used in this paper. Centers of inclusions are represented by vertices of triangles. In the figure, d represents the nearest neighbor distance for one pair of inclusions, α represents the angle to nearest neighbor for one pair of inclusions, A_p represents

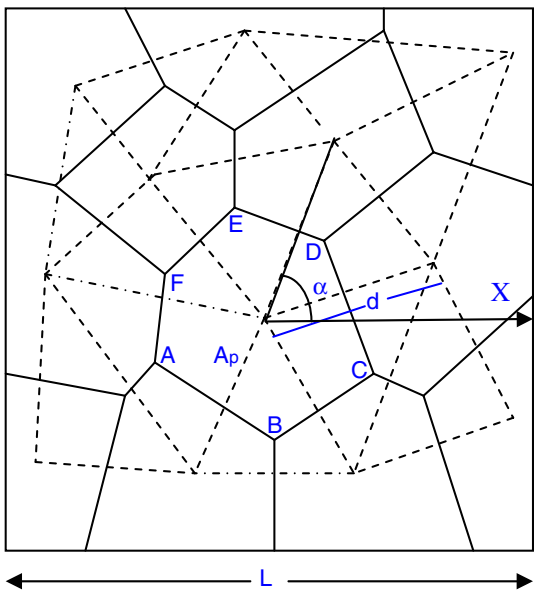

Fig. 2 Schematic of statistical descriptors

the area of one individual polygon, A_{SVE} represents the area of the SVE and N represents the nearest neighbors (e.g., the number of polygons surrounding the inclusion/polygon under consideration). For instance, for the polygon *ABCDEF* there are six polygons which share a polygon boundary *AB, BC,..., FA*. Hence the number of nearest neighbors is six, similarly the number of nearest neighbors can be computed for all the polygons under consideration. L is the length of the SVE.

Statistical characterization of microstructure morphology

In this paper two types of random arrangements are presented:

- Random arrangement of carbon-epoxy composites of selected actual samples obtained from different patches of composites.
- Random arrangement of model composite generated numerically.

Random arrangement of carbon-epoxy composites of selected actual samples

In this study, three samples of composite made of AS4 carbon fiber and epoxy matrix, which were obtained from three different patches of composites, were evaluated. We refer to these samples as set#1, set#2 and set#3. About 50 SVEs were obtained from each set. Figure 3 shows examples of SVEs obtained from the three sets considered. For complete list of all SVEs please see [41]. Each SVE was digitized and image processing was used to locate the center of each fiber. The coordinate of the fibers within each SVE were used as seeds to locate the vertices of Delaunay triangles. For each sample, values of the following *statistical descriptors* were calculated: nearest neighbor distance; nearest neighbor angle; cell size (area of Voronoi cell); and number of nearest neighbors. Various Probability Distribution Functions (*PDF*s) were used and for each descriptor, the cumulative probability distribution (CPD) was calculated according to [40–51]. Kolmogorov–Smirnov test (KS-test) was, then, used to determine the best fit for each set [40–51].

Probability distribution fits of the four statistical descriptors for set #1 with 234 inclusions are shown in Fig. 4. Five different fits were used to fit the data. Namely: uniform, normal (Gaussian), Weibull, β and γ. For set #1, all probability distribution functions except the uniform distribution fit the experimentally obtained data as indicated by the KS-test. Similar curves were generated for the other two sets [41]. This technique may be used as quality check for the dispersion of inclusion. For example, the gradual increase in the cumulative probability distribution in Fig. 4 indicates that the inclusions in the data set#1 are distributed randomly with very little clustering. On the other hand, by examining Fig. 5 which shows a comparison of the distribution of separation distances for three data sets, it is fair to say that both data sets #2 and #3 have a predominant

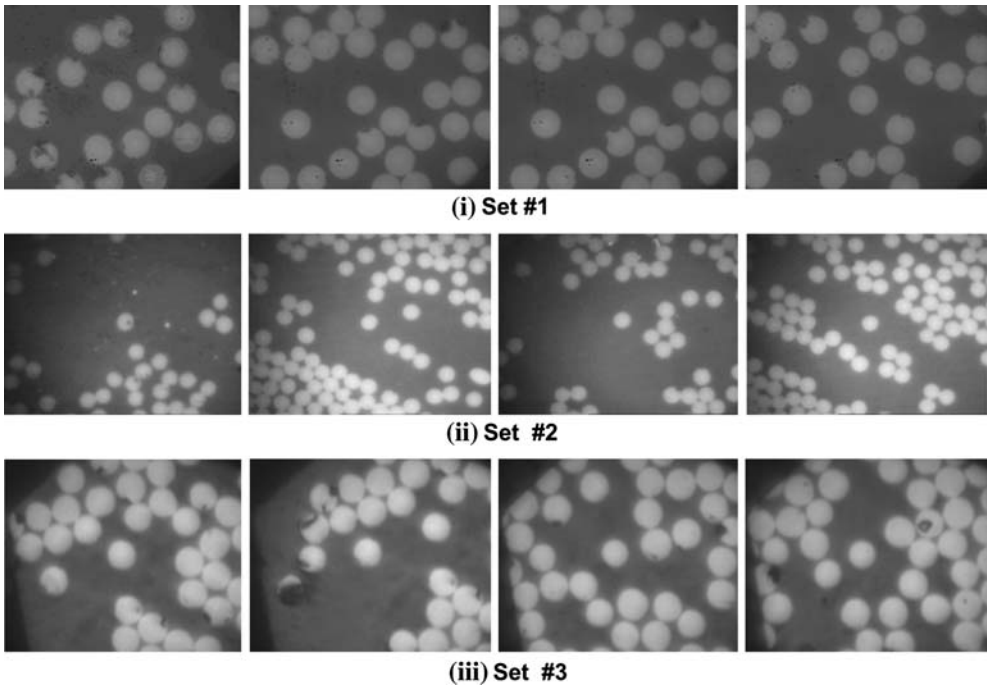

Fig. 3 Example of SVEs obtained from experimental sets #1, #2 and #3

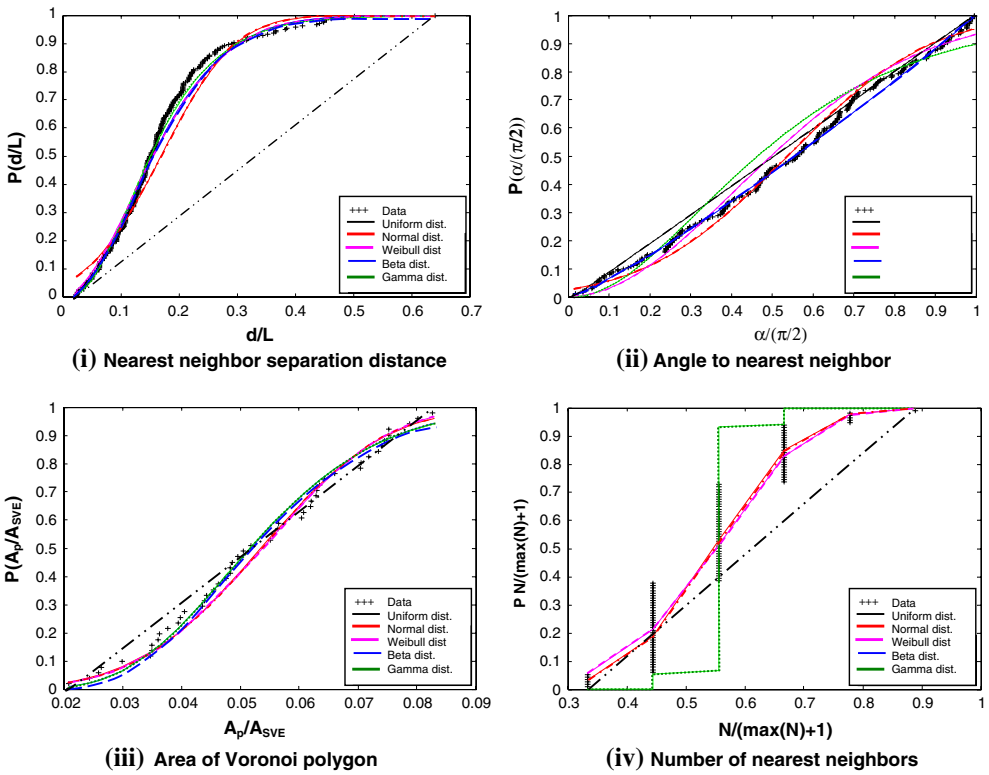

Fig. 4 Probability distribution fits of the four statistical descriptors for the data obtained from experimental set #1

clustering as compare to data set #1. The same has been observed for the rest of the statistical descriptors.

The K-test may be used to differentiate between different composite processing procedures. This may be achieved by comparing the CPD of the composite under consideration with standard distribution curves of ideal or required composite which will be more informative than looking to the average (μ), standard of deviation (σ) or coefficient of variation (COV). For example the overall statistic information about distribution of fibers in the three sets that are shown in Table 1 can give very little information on the actual distribution of these fibers.

The relation between the nearest neighbor distance (d) and the area of Voronoi polygon A_p for the data obtained from set #1 is shown in Fig. 6 which shows a strong correlation between the distance to nearest neighbor and size of Voronoi polygon. It shows that the closer the distance between neighboring inclusions the smaller the generated Voronoi cell area will be. Thus, it is expected that the stress concentration will increase as the size of Voronoi cell decreases.

Random arrangement of model composite generated numerically

In this paper we, also, used numerical generation of random fiber locations to optimize the number of SVEs needed to fully describe random microstructure. Overall statistical parameters (e.g., μ and σ for normal distribution, κ and λ for Gamma distribution ...etc) were chosen to be the same as those obtained from the limited experimental observations described in Section ''Random arrangement of carbon-epoxy composites of selected actual samples'' according to the relations shown in Appendices 1 and 2. Also, we used numerical generation of random fiber location to characterize clustering using statistical descriptors.

Effect of number of SVE on statistical descriptors

The window concept is introduced as a square-shaped domain taken from the random medium $B(\omega)$. The window size is introduced as:

$$\delta = \frac{L}{d} \tag{2}$$

This defines a non-dimensional parameter δ typically greater than 1, specifying the scale L of observation (or measurement) relative to typical micro scale d (i.e. crystal or inclusion size) of the material microstructure. The window may be placed arbitrary in the domain of $B(\omega)$ with smallest size $\delta > 1$ (i.e. the scale of crystal or inclusion). Since for any $\delta > 1$, B_δ is a random rather than a deterministic medium, the window of size δ plays the role of a SVE of the continuous random medium model [57].

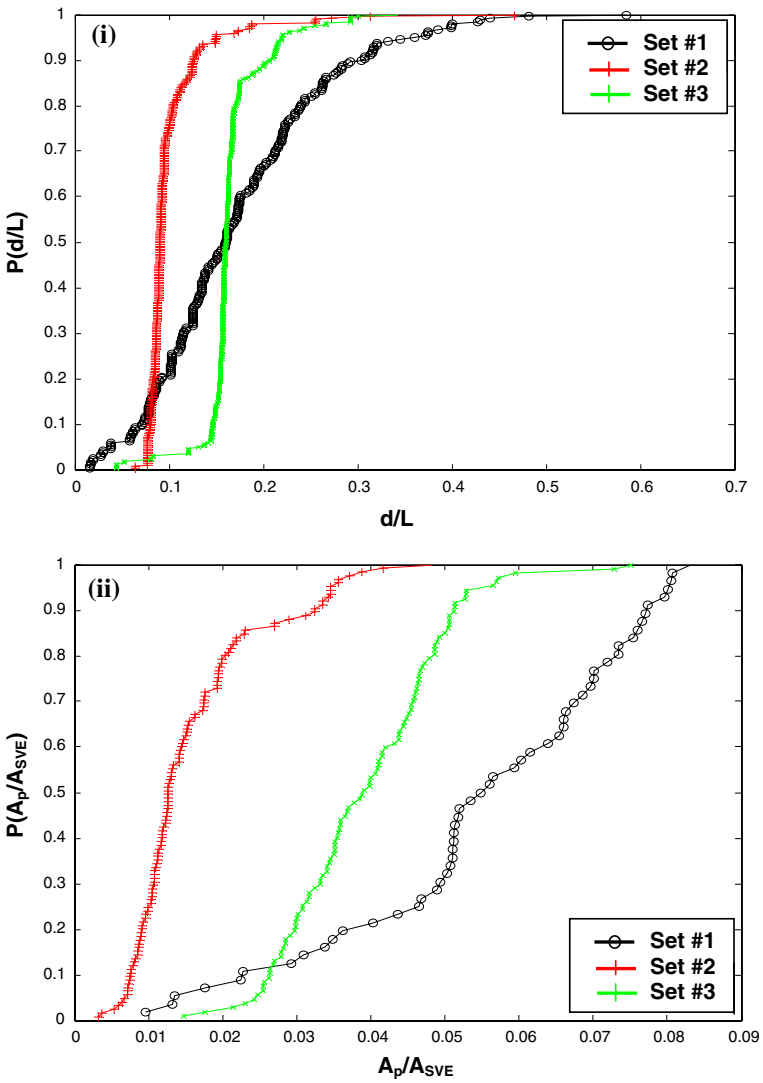

Fig. 5 Comparison of probability distribution of (i) nearest neighbor distance and (ii) area of Voronoi cells for three data sets obtained from three different samples

Table 1 Overall statistics for the experimental data

		μ	σ	COV
Set #1	Nearest neighbor distance	0.1632	0.08	2.04
	Angle to nearest neighbor	46.1885	26.1592	1.765669439
	Size of cell	0.0892	0.0832	1.072115385
	# nearest neighbors	4.9151	1.0521	4.671704211
Set #2	Nearest neighbor distance	0.1004	0.0373	2.691689008
	Angle to nearest neighbor	46.4755	27.1845	1.709632327
	Size of cell	0.0397	0.0723	0.549100968
	# nearest neighbors	5.527	1.0791	5.12186081
Set #3	Nearest neighbor distance	0.1651	0.034	4.855882353
	Angle to nearest neighbor	45.2076	28.2002	1.603095014
	Size of cell	0.0394	0.0253	1.557312253
	# nearest neighbors	5.2267	0.9617	5.434854944

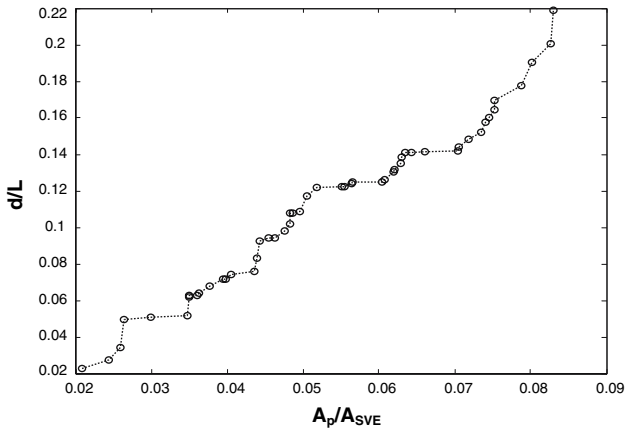

Fig. 6 Correlation between nearest neighbor distance and size of polygon for the data obtained from set #1

The requirements and methods of evaluating SVEs have been discussed in detail by [52–56]. In order to have a representative volume element (RVE) that represents an infinite microstructure, one needs to have a very large SVE. This may be limited by the computational power used. Alternatively, one can use many realizations of smaller SVEs [57]. In this paper, many realizations of a relatively small SVE were used to get the required accuracy. Keeping in mind that the volume fraction (v_f) may be different from one SVE to another as shown in Fig. 7, a variation in the volume fraction was introduced in accordance to the following relation:

$$v_f = \langle v_f \rangle \left(1 + \frac{r}{100}\right) \tag{3}$$

where r = random number (we used Poisson distribution). Also, we used r = [–10, 10] or [–30, 30], $\langle v_f \rangle = 0.55$.

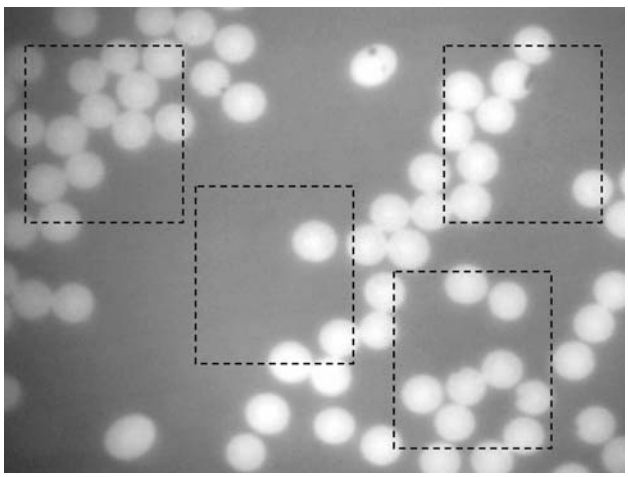

Fig. 7 Schematic showing that the morphology and volume fraction may be different for different SVEs obtained from the same sample and of same size

Figure 8 shows the COV of statistical parameters versus the number of SVEs. Theoretically speaking, as the number of SVEs approaches infinity the value of COV of statistical descriptors becomes constant and we will have an RVE. For this case of study, at around 100 realizations; the COV of all statistical descriptors converge to constant values for all of the three cases (constant volume fraction, with ±10% variation in volume fraction, and with ± 30% variation in volume fraction). Thus, only 100 realizations are needed to get statistically meaningful representation of the microstructure.

Effect of clustering

Another way of classification of microstructure randomness may be defined in which the geometric disorder is divided into a hardcore model and a cluster model. The hardcore model is obtained by imposing certain prohibitive distance (i.e., a minimum distance between the points in the microstructure). Clustering in composites can be due to many reasons (i.e., electromagnetic attraction in nano-scale materials). In order to simulate clustering, parent points were generated and distributed randomly in a hard core model within an SVE. Then, off-spring points were distributed around parent point. The off-spring points were distributed randomly with either a constant number of points (we refer to this as uniform clustering) or with a variable number of points (we refer to this as random clustering). Gaussian distribution was used to generate all the points. The total number of points was kept constant and the following cases were investigated: random clustering with 10 parent points; uniform clustering with 10 parent points; random clustering with 20 parent points; and uniform clustering with 20 parent points Fig. 9 shows the four clustering cases where the total number of off-spring points was kept at a constant value of 1,000 with either constant or variable number of off-spring points associated with each parent point. For example, for the case of random clustering with 10 parent points , the number of off-spring points associated with parent points was varied randomly between 40 and 220.

Typical CPD curves of the four statistical descriptors for the case of random clustering with 10 parent points are shown in Fig. 10.

Correlating detailed microstructure morphology to local elastic fields

In this paper, the inclusions and the matrix are assumed to be two distinct homogeneous isotropic materials. As a result we have a realistic ergodic model without holes or rigid inclusions described by a random field

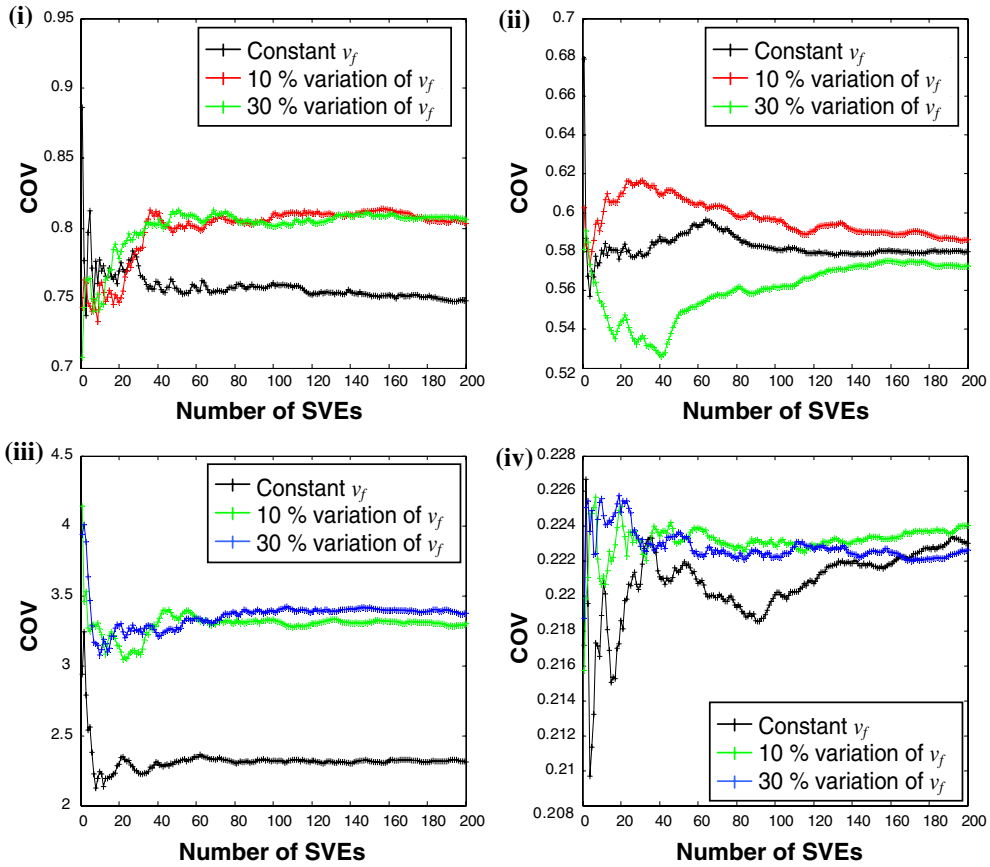

Fig. 8 Effect of number of SVEs on COV of (i) distance to nearest neighbor, (ii) angle to nearest neighbor, (iii) size of Voronoi cell, and (iv) number of nearest neighbors for cases of 0%, 10% and 30% random variation of volume fraction

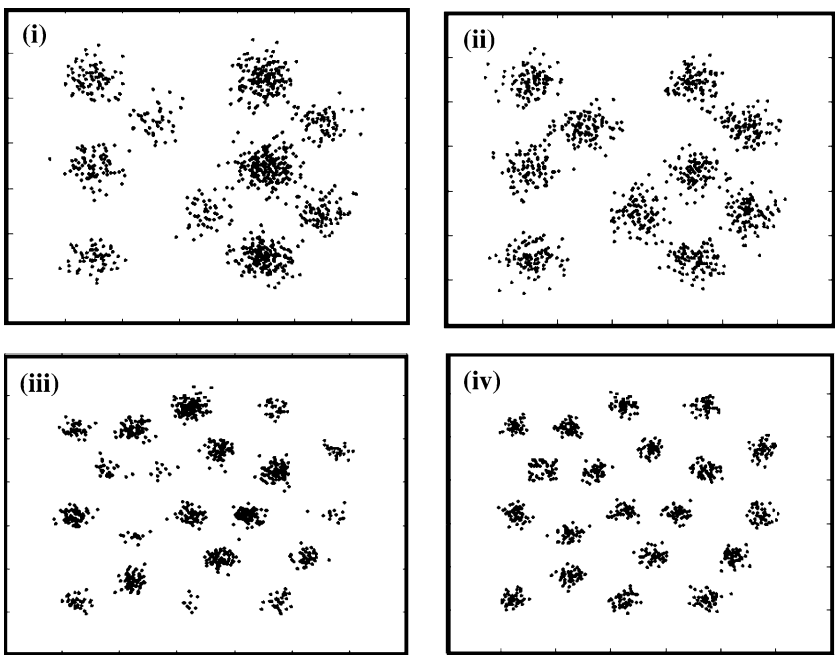

Fig. 9 (i) Random clustering with 10 parent points, (ii) uniform clustering with 10 parent points, (iii) random clustering with parent points, and (iii) uniform clustering with 20 parent points

$C = \{C(x,\omega); x \in B; \omega \in \Omega\}$ with piecewise-constant realizations.

To create a non-uniform arrangement of inclusions, random numbers, indicating centers of inclusions were generated according to planar Poisson's distribution. We imposed restriction that the inclusions do not overlap. We used the commercially available finite element package ANSYS 7.0 [58]. We utilized quadrilateral plane stress

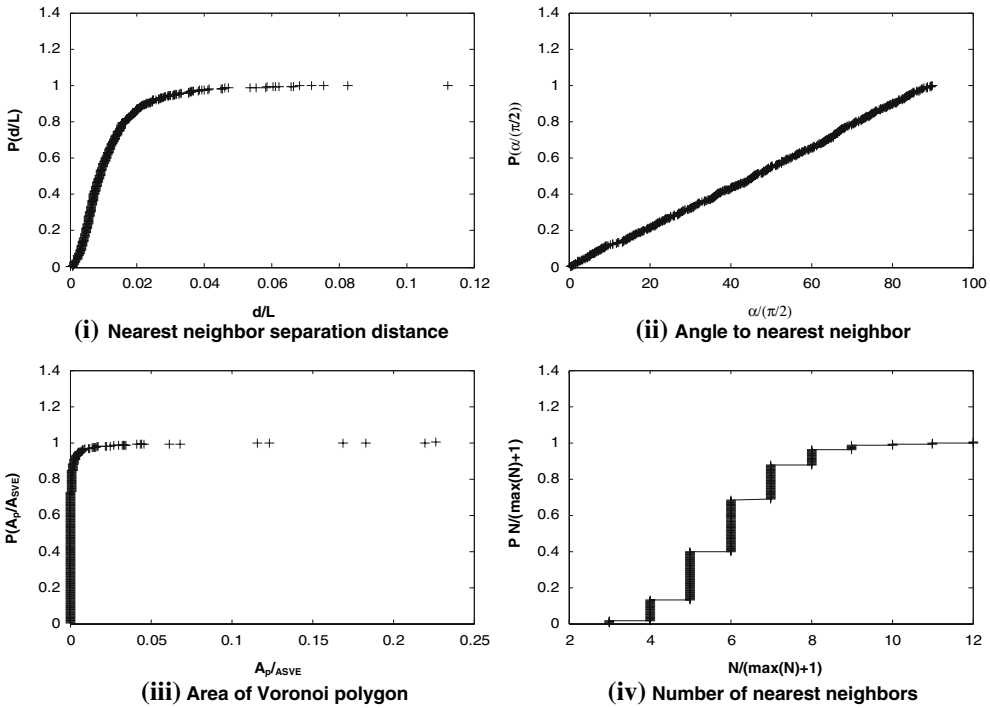

Fig. 10 Probability distribution of the four statistical descriptors for random clustering with 10 parent points

elements; such that each element was define by four nodes having two degrees of freedom: translation in the nodal x_1 and x_2 directions and we used plane stress condition. Four cases were evaluated:

- 500 inclusions with $\langle v_f \rangle = 0.245$, and $\delta = \frac{L}{d} = \frac{1}{0.0125} = 80$
- 100 inclusions with $\langle v_f \rangle = 0.245$, and $\delta = \frac{L}{d} = \frac{1}{0.0025} = 40$
- 100 inclusions with $\langle v_f \rangle = 0.05$, and $\delta = \frac{L}{d} = \frac{1}{0.0125} = 80$
- 100 Voronoi polycrystals using the method of homogenization

where v_f is the volume fraction of inclusions.

Two types of boundaries of the square microstructure window were imposed ∂B^1_δ and ∂B^2_δ where the superscripts indicate the outer normal (Fig. 11).

The window was subjected to kinematic boundary conditions on ∂B^2_δ

$$u(x+L) = u(x) + \varepsilon^0 \cdot x \quad \forall x \in B^1_\delta \tag{4}$$

and periodic boundary conditions on ∂B^1_δ

$$\begin{aligned} u(x+L) &= u(x) \\ t(x+L) &= -t(x) \end{aligned} \quad \forall x \in B^2_\delta \tag{5}$$

where u is the displacement at x, ε^0 is applied strain, t is surface traction. Also, $L = Le$ with e being a unit vector.

The composite that was simulated was AS4-carbon fibers randomly dispersed in an epoxy matrix. Properties for the matrix and the fiber used in this paper are shown in Table 2. Discrete properties were given for corresponding

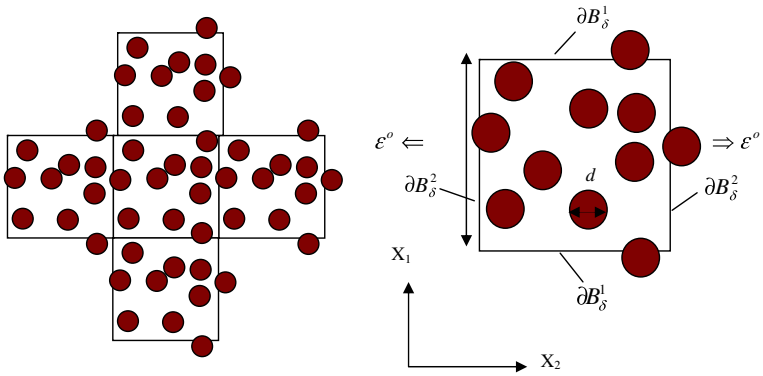

Fig. 11 An RVE of a periodic window of scale $\delta = L/d$ for the case of disordered matrix–inclusion composite of periodicity L showing a schematic of the applied loading used in the FEA

Table 2 Elastic properties of carbon/epoxy constituents used

Material	Young's modulus, GPa (Msi)	Poisson's ratio	CTE (μm/m/°C)	TG, °C (°F)
AS4 carbon fiber	221 (32)	0.25	1.6	
Epoxy matrix	3.0 (0.44)	0.38	194	75 (167)

regions of fibers and matrix. Each window was subjected to the boundary conditions described in Eqs. 4 and 5.

Contour plots of von Misses stresses $(\sigma_{\text{eff}}^{\text{m}})$ in the matrix, for the first three cases considered, are shown in Fig. 12. In all cases a constant strain of $\varepsilon^0 = 0.01$ was applied in the horizontal direction. This applied strain is equivalent to an average stress $(\bar{\sigma})$ of 7427 psi for the first two cases and 5,116 psi for the third case. The contour plots illustrate the effect of random arrangement of inclusions on distribution of stresses around reinforcing inclusions. Observe that the stresses are distributed very unevenly between inclusions. This is in contrast of periodic arrangements in which inclusions share the same a mount of loading equally. The rotation of the plots in Fig. 12 is due to rigid body displacement associated with the resulting non-uniform displacement field at the edge of the RVE. This non-uni-from displacement is due to the random arrangement of inclusions.

In order to evaluate the distribution of stresses, probability distribution fits were used. Figure 13 shows the cumulative probability distribution of the maximum von Misses stresses in the matrix around each inclusion for all three cases. Three PDF were used to fit the data: Weibull, Normal and Gamma. Using the Kolmogorov–Smirnov test (KS-test), it was found that, for these cases, all the three distributions fit the $\sigma_{\text{eff}}^{\text{m}}$ data.

From Fig. 12 one can observe that there is some kind of bridging effect of stresses between inclusions in the direction of applied loading. Inclusions that are closer to each other tend to produce higher stress in the matrix. This effect is demonstrated in Figs. 14 and 15 were the maximum stress around each inclusion is correlated to the separation distance to closest neighboring inclusion and to the size of resulting Voronoi cell for the case of 500 inclusions with $\langle v_f \rangle = 0.245$. It is clear that the smaller the size of the Voronoi cell and the smaller the separation distance between inclusions, the larger the associated stress is. Thus, this may indicate an earlier possibility of fracture under a given load for composites with high degree of clustering. Similar behavior was observed for the other three cases [41].

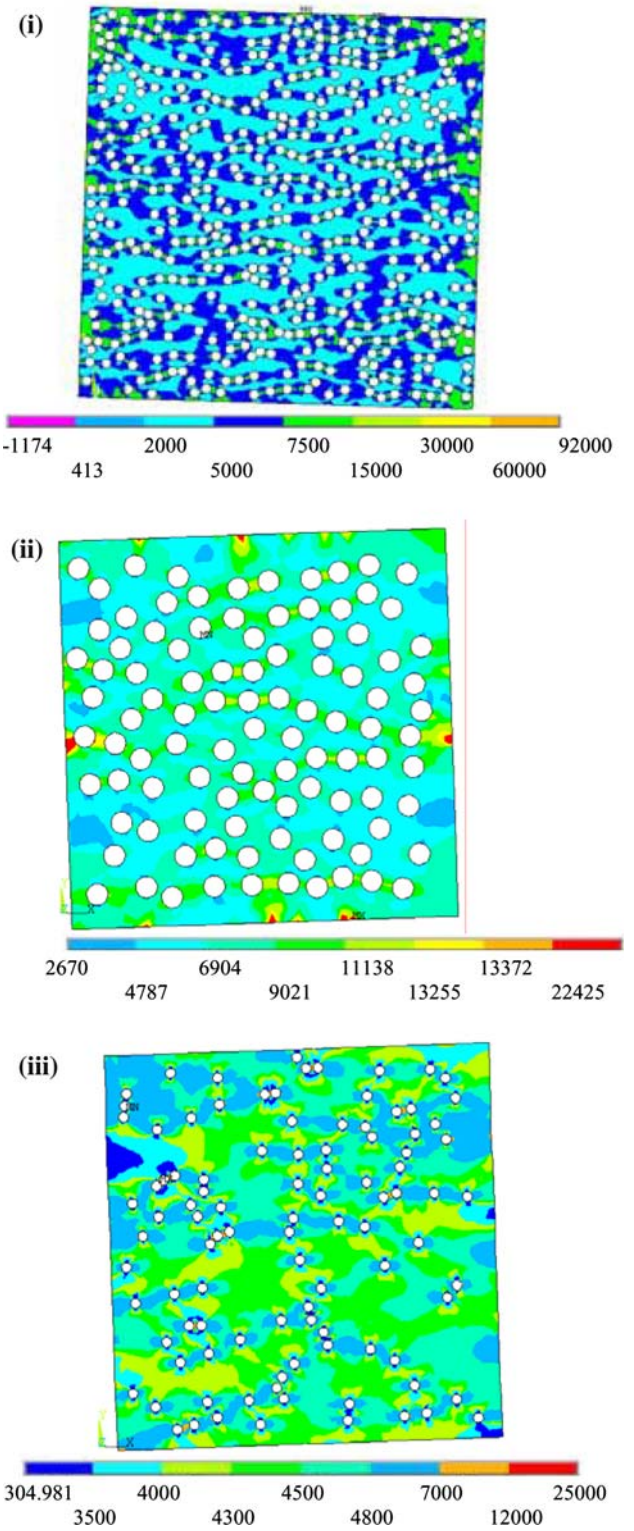

Fig. 12 Contour plots of $\sigma_{\text{eff}}^{\text{m}}$ (psi) for the case of (i) 500 inclusions with $\langle v_f \rangle = 0.245$, (ii) 100 inclusions with $\langle v_f \rangle = 0.245$, and (iii) 100 inclusions with $\langle v_f \rangle = 0.05$ subjected to uniaxial strain $\varepsilon^0 = 0.01$ in the x-direction

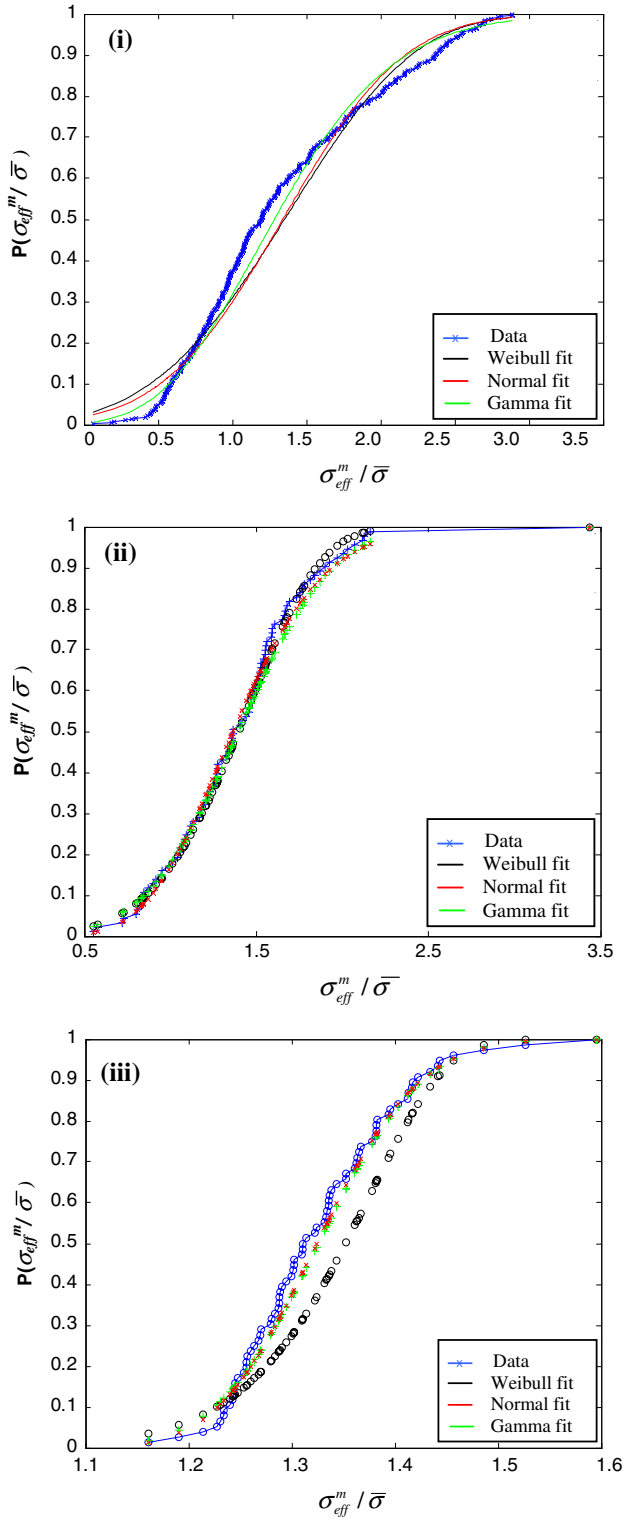

Fig. 13 Probability distribution $\sigma_{\text{eff}}^{\text{m}}$ for (i) 500 inclusions with $\langle v_f \rangle = 0.245$, (ii) 100 inclusions with $\langle v_f \rangle = 0.245$, and (iii) 100 inclusions with $\langle v_f \rangle = 0.05$ for cases of a uniaxial applied strain of $\varepsilon^0 = 0.01$

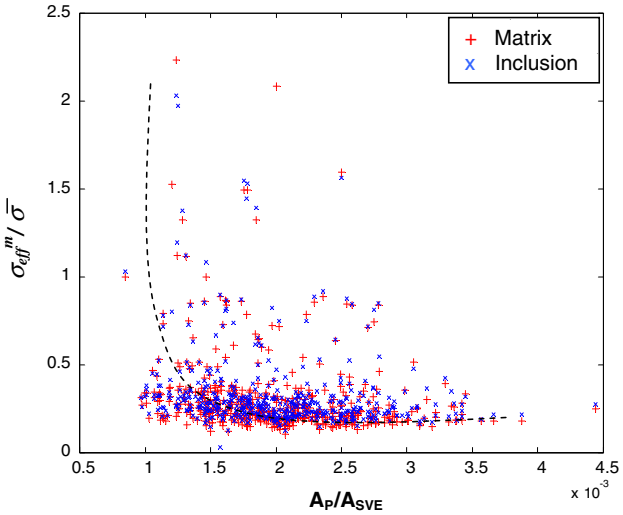

Fig. 14 Effect of size of Voronoi cell on maximum $\sigma_{\text{eff}}^{\text{m}}$ in each cell for the case of 500 inclusions with $\langle v_f \rangle = 0.245$

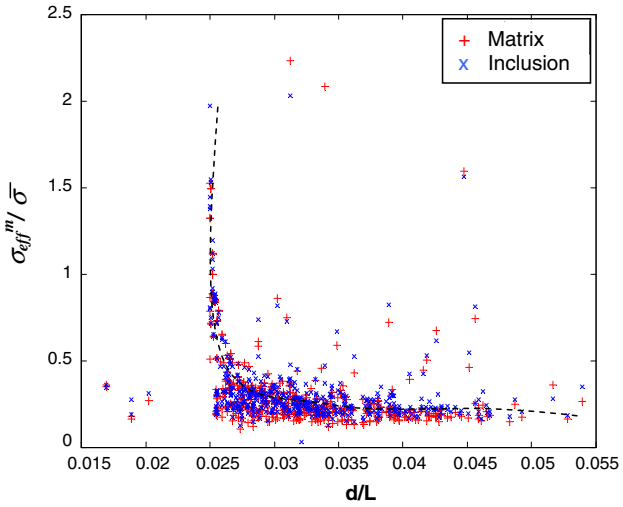

Fig. 15 Effect of separation distance to nearest neighbor on maximum $\sigma_{\text{eff}}^{\text{m}}$ in each cell for the case of 500 inclusions with $\langle v_f \rangle = 0.245$

Homogenization

Effective medium theories had been used to estimate homogenized properties of composite materials and average stresses. For review see [59–63]. The case of 100 inclusions with total volume fraction of 0.05 was evaluated and Voronoi cells were drawn around each inclusion. Local volume fractions were calculated for each cell and elastic properties were obtained using self consistent and composite cylinder models for transversely isotropic materials

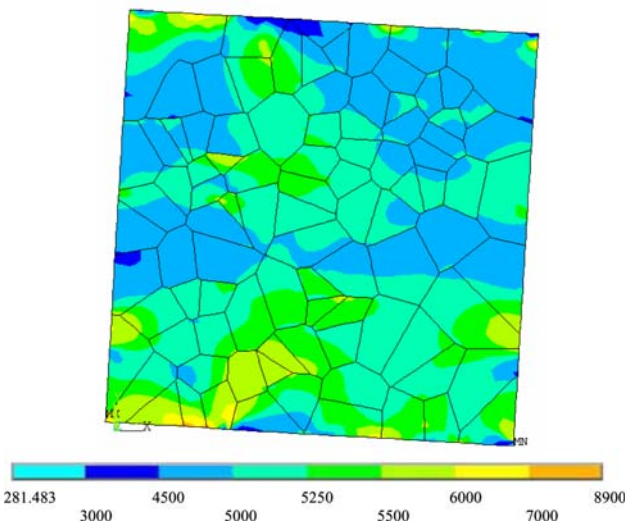

Fig. 16 Contours of σ^{p}_{eff} (psi) for homogenized polygons

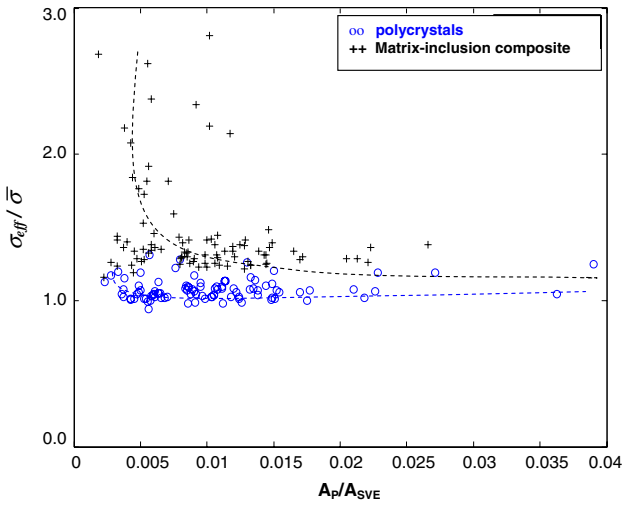

Fig. 18 Effect of size of Voronoi cell on maximum σ^{m}_{eff} and σ^{p}_{eff} in each cell

[63] to homogenize elastic properties within each Voronoi cell (see Appendix 3). Thus, polycrystalline structure was constructed.

Finite element method was used to obtained contour plot of calculate the distribution of σ^{p}_{eff} (Fig. 16). Note that the stress distribution is more uniform in this case as compared to the case shown in Fig. 12 (iii). The rotation of the plots is due to rigid body displacement associated with the relatively non-uniform displacement field at the edge of the RVE. Figure 17 shows the CPD of the von Mises stress in the homogenization case (σ^{p}_{eff}) and the 100 inclusions case (σ^{m}_{eff}). From the probability distribution graph it can be seen that the stresses in the homogenization case are more

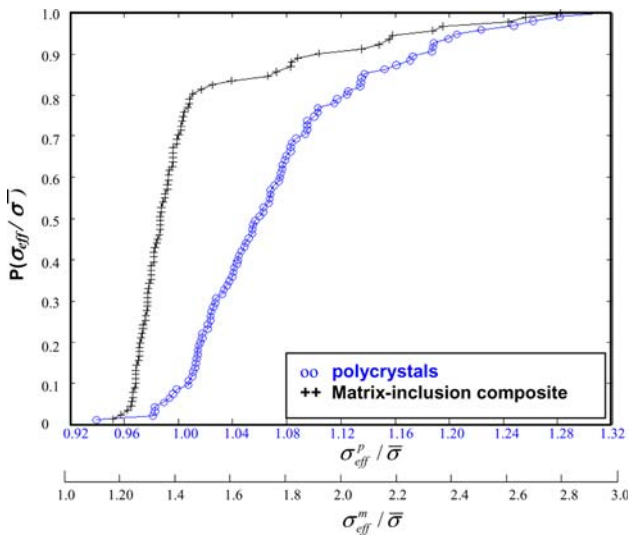

Fig. 17 Probability distribution of σ^{m}_{eff} and σ^{p}_{eff} for case of matrix inclusion composite and for polycrystals case

Table 3 Mean, standard of deviation and coefficient of variation of σ^{m}_{eff} for all the four cases

	μ (ksi)	σ (ksi)	COV
500 inclusions $\langle v_f \rangle = 0.245$, $\delta = 80$	8.2 E+03	1.2 E+04	0.683
100 inclusions $\langle v_f \rangle = 0.245$, $\delta = 35.8$	8.68 E+03	2.5 E+03	0.285
100 inclusions $\langle v_f \rangle = 0.05$, $\delta = 80$	7.83 E+03	3.97 E+03	0.5075
Homogenization $\langle v_f \rangle = 0.05$	5.374 E+03	354.25	0.0659

confined to a smaller range of values with a more gradual increase in compare to the case of 100 inclusions (composite) of the same volume fraction and distribution. Also the effect of polygon size on maximum stress in each cell is more pronounced for the case of the 100 inclusion (Fig. 18). As it is evident from Fig. 18, the von Mises stress in the composite is always higher than the homogenization case. Thus homogenization method undermines the maximum stresses in composites. Table 3 shows the overall statistics of the distribution of σ_{eff} for all four cases considered in this paper. Note that by fixing the volume fraction and reducing the number of inclusion, the COV of σ_{eff} will be much smaller. This is due to the fact that, the larger the number of the inclusion, the larger the probability of inclusions to be at a closer distance from one another. Also, the table shows that the stresses in the homogenized composite (polycrystals case) are much more uniform than that of equivalent case of randomly distributed inclusions.

Conclusions

This paper sets a frame work for correlating microstructure morphology of random inclusion–matrix composites to their local stress fields. It is shown that Voronoi cells and Delaunay triangulation may serve as a sound technique for characterizing random microstructure of various composites. This technique may be used as a quality control approach for statistical characterization of different classes of composites (e.g., identifying degree of clustering). Based on the groundwork laid in this paper, one may use the same approach to study the effect of random interphase or interface, random shape and random size of inclusions.

Acknowledgements The authors wish to acknowledge the partial support for this research from U.S. Air Force Grant # F08637-03-C-6006 with a subcontract # S-29000.23 from Applied Research Associates Inc. Also, the authors would like to acknowledge the collaboration and help they received from Prof. Martin Ostoja-Starzewski.

Appendix 1 Mean and standard deviation of probability distributions

Distribution name	Mean	Standard deviation
Normal	μ	σ
Lognormal	$\exp\left(\lambda+\frac{\zeta^2}{2}\right)$	$\exp\left(\lambda+\frac{\zeta^2}{2}\right)\left[\exp(\zeta^2-1\right]^{1/2}$
Gamma	$\frac{k}{\lambda}$	$\frac{\sqrt{k}}{\lambda}$
Shifted Rayleigh	$v_0+\left(\frac{\pi}{2}\right)^{1/2}\alpha$	$\left(2-\frac{\pi}{2}\right)^{1/2}\alpha$
Shifted exponential	$v_0+\frac{1}{\lambda}$	$\frac{1}{\lambda}$
Uniform	$\frac{a+b}{2}$	$\frac{b-a}{2\sqrt{3}}$
Beta	$a+\frac{q(b-a)}{q+r}$	$\frac{b-a}{q+r}\left(\frac{qr}{q+r+1}\right)^{1/2}$
Type I largest value	$u_n+\frac{0.5772}{\alpha_n}$	$\frac{\pi}{\sqrt{6\alpha_n}}$
Type I smallest value	$u_1-\frac{0.5772}{\alpha 1}$	$\frac{\pi}{\sqrt{6\alpha_1}}$
Type II largest value	$u_n\Gamma\left(1-\frac{1}{k}\right)$	$u_n\left[\Gamma\left(1-\frac{2}{k}\right)-\Gamma^2\left(1-\frac{1}{k}\right)\right]^{1/2}$
Type III smallest value	$\varepsilon+(u_1-\varepsilon)\Gamma\left(1+\frac{1}{k}\right)$	$(u_1-\varepsilon)\left[\Gamma\left(1+\frac{2}{k}\right)-\Gamma^2\left(1+\frac{1}{k}\right)\right]^{1/2}$

Appendix 2 Probability distribution library

Distribution name	Id	PDF, $f_x(x)$	CDF, $F_x(x)$	Parameters				note
				P_1	P_2	P_3	P_4	
Normal	1	$\frac{1}{\sqrt{2\pi}\sigma}\exp\left[\frac{-1}{2}\left(\frac{x-\mu}{\sigma}\right)\right]$	$\Phi\left[\frac{x-\mu}{\sigma}\right]$	μ	$0<\sigma$			1
Lognormal	2	$\frac{1}{\sqrt{2\pi}\zeta x}\exp\left[\frac{-1}{2}\left(\frac{\ln x-\lambda}{\zeta}\right)^2\right]$	$\Phi\left[\frac{\ln x-\lambda}{\zeta}\right]$	λ	$0<\zeta$			1
Gamma	3	$\frac{\lambda(\lambda x)^{k-1}}{\Gamma(k)}\exp(-\lambda x), 0\leqslant x$	$\frac{\Gamma(k,\lambda x)}{\Gamma(k)}$	$0<\lambda$	$0<k$			2,3
Shifted exponential	4	$\lambda\exp[-\lambda(x-x_0)], x_0\leqslant x$	1–exp $(-\lambda\ (x–x_0))$	$0<\lambda$	x_0			
Shifted Rayleigh	5	$\frac{(x-x_0)}{\alpha^2}\exp\left[\frac{-1}{2}\left(\frac{x-x_0}{\alpha}\right)^2\right], x_0\leqslant x$	$1-\exp\left[\frac{-1}{2}\left(\frac{x-x_0}{\alpha}\right)^2\right]$	a	x_o			
Uniform	6	$\frac{1}{(b-a)}, a\leqslant x\leqslant b$	$\frac{x-a}{b-a}$	a	b			
Beta	7	$\frac{(x-a)^{q-1}(b-x)^{r-1}}{B(q,r)(b-a)^{q+r-1}}, a\leqslant x\leqslant b$		$0<q$	0 < r	a	b	4
Type I larget value	11	$\alpha_n\exp\ [\ -\alpha_n\ (x–u_n\ )–\ \exp\ (-\alpha_n\ (x–u_n\ )\ )\ ]$	$\exp\ [\ -\exp\ (-\alpha_n\ (x–u_n\ )\ )\ ]$	u_n	$0<\alpha_n$			5
Type I smallest value	12	$\alpha_1\exp\ [\ \alpha_1\ (x–u_1\ )–\ \exp\ (\alpha_1\ (x–u_1\ )\ )\ ]$	1–exp $[\ -\exp\ (\alpha_1\ (x–u_1\ )\ )\ ]$	u_1	$0<\alpha_1$			
Type II largest value	13	$\frac{k}{u_n}\left(\frac{u_n}{x}\right)^{k+1}\exp\left[-\left(\frac{u_n}{x}\right)^k\right], 0<x$	$\exp\left[-\left(\frac{u_n}{x}\right)^k\right], 0<x$	u_n	$0<k$			
Type III smallest value	14	$\frac{k}{u_1-\varepsilon}\left(\frac{x-\varepsilon}{u_1-\varepsilon}\right)^{k-1}\exp\left[-\left(\frac{x-\varepsilon}{u_1-\varepsilon}\right)\right], \varepsilon\leqslant x$	$1-\exp\left[-\left(\frac{x-\varepsilon}{u_1-\varepsilon}\right)^k\right]$	u_1	$0<k$			6

Note:

1. $\Phi(x)=(2\pi)^{-1}\int_{-\infty}^{x}\exp(-u^2/2)\mathrm{d}u$ is the standard normal cumulative probability
2. $\Gamma(k)=\int_0^\infty e^{-u}u^{k-1}\mathrm{d}u$ is the gamma function. For integer k, $\Gamma(k)=(k-1)!$
3. $\Gamma(k,x)=\int_0^x e^{-u}u^{k-1}\mathrm{d}u$ is the incomplete gamma function with $\Gamma\ (k,\infty\ )=\Gamma\ (k\ )$
4. $B(q,r)=\frac{\Gamma(q)\Gamma(r)}{\Gamma(q+r)}$ is the beta function
5. This distribution is also known as Gumbel distribution
6. For $\varepsilon=0$, this distribution if known as the Weibull distribution

Appendix 3: Self Consistent method [62]

Consider a system of aligned fibers along the x_1 direction. Media of this type have symmetry properties in the plane normal to the fiber direction (x_2 x_3 directions). Such media are characterized as transversely isotropic materials. Such media have five independent constants (i.e. (i.e. $E_{11}, v_{12}, K_{23}, \mu_{12}, \mu_{23}$). Where E, K and μ are the Young's, bulk and shear modulii respectively and v is the Poisson's ratio.

$$E_{11}=(1-f)E_m+fE_f + \frac{4f(1-f)(v_f-v_m)^2\mu_m}{[(1-f)\mu_m/(K_f+\mu_f/3)]+[f\mu_m/(K_m+\mu_m/3)]+1} \tag{A1}$$

$$\mu_{12}=(1-f)v_m+fv_f + \frac{f(1-f)(v_f-v_m)[\mu_m/(K_m+\mu_m/3)-\mu_m/(K_f+\mu_f/3)]}{[(1-f)\mu_m/(K_f+\mu_f/3]+[f\mu_m/(K_m+\mu_m/3)]+1} \tag{A2}$$

$$K_{23}=K_m+\frac{\mu_m}{3} + \frac{f}{1/[K_f-K_m+\frac{1}{3}(\mu_f-\mu_m)]+(1-f)/\left[K_m+\frac{4\mu_m}{3}\right]} \tag{A3}$$

$$\frac{\mu_{12}}{\mu_m}=\frac{\mu_f(1+f)+\mu_m(1-f)}{\mu_f(1-f)+\mu_m(1+f)} \tag{A4}$$

$$A\left(\frac{\mu_{23}}{\mu_m}\right)^2+2B\left(\frac{\mu 23}{\mu_m}\right)+C=0 \tag{A5}$$

where

$$\begin{aligned}
A&=3f(1-f)^2\left(\tfrac{\mu_f}{\mu_m}-1\right)\left(\tfrac{\mu_f}{\mu_m}=\eta_f\right)\\
&\quad+\left[\tfrac{\mu_f}{\mu_m}\eta_m+\eta_f\eta_m=\left(\tfrac{\mu_f}{\mu_m}-\eta_f\right)f^3\right]\\
&\quad*\left[f\eta_m\left(\tfrac{\mu_f}{\mu_m}-1\right)-\left(\tfrac{\mu_f}{\mu_m}\eta_m+1\right)\right]\\
B&=3f(1-f)^2\left(\tfrac{\mu_f}{\mu_m}-1\right)\left(\tfrac{\mu_f}{\mu_m}=\eta_f\right)\\
&\quad+\tfrac{1}{2}\left[\tfrac{\mu_f}{\mu_m}\eta_m+\left(\tfrac{\mu_f}{\mu_m}-1\right)f+1\right]\\
&\quad*\left[(\eta_m-1)\left(\tfrac{\mu_f}{\mu_m}\eta_m+\eta_f\right)-2\left(\tfrac{\mu_f}{\mu_m}\eta_m-\eta_f\right)f^3\right]\\
&\quad+\tfrac{f}{2}(\eta_m+1)\left(\tfrac{\mu_f}{\mu_m}-1\right)\left[\left(\tfrac{\mu_f}{\mu_m}\eta_m+\eta_f\right)+\left(\tfrac{\mu_f}{\mu_m}\eta_m-\eta_f\right)f^3\right]\\
C&=3f(1-f)^2\left(\tfrac{\mu_f}{\mu_m}-1\right)\left(\tfrac{\mu_f}{\mu_m}+\eta_f\right)\\
&\quad+\left[\tfrac{\mu_f}{\mu_m}\eta_m+\left(\tfrac{\mu_f}{\mu_m}-1\right)f+1\right]\\
&\quad*\left[\tfrac{\mu_f}{\mu_m}\eta_m+\left(\tfrac{\mu_f}{\mu_m}\eta_m-\eta_f\right)f^3\right]
\end{aligned} \tag{A6}$$

where f = Volume fraction η = 3–4v.

References

1. Eshelby JD (1957) Proc Roy Soc A241:376
2. Mori T, Wakashima K (1990) In: Weng GJ, Taya M, Abe H (eds) Micromechanics and inhomogeneity, the Mura Anniversary volume. Springer, New York, 269 pp
3. Benveniste G, Dvorak G, Chen T (1989) Mech Mater 7:305
4. Tong Y, Jasiuk I (1990) In: Proc. American Society for composites. 5th technical conference, Technomic, Lancaster, PA, p 117
5. Nemat-Nasser S, Hori M (1999) Micromechanics: overall properties of heterogeneous materials, 2nd edn. Amsterdam, North-Holland
6. Chen J, Thorpe M, Davis L (1995) J Appl Phys 77:4349
7. Takao Y, Taya M, Chou T (1982) J Appl Mech 49:536
8. AL-Ostaz A, Jasiuk I (1997) Acta Mater 45(10):4131
9. Becker R, Smelser REJ (1994) J Mech Phys Solids 42:773
10. Brockenbrough JR, Suresh S, Wienecke HA (1991) Acta Metal Mater 39:735
11. Alzebdeh K, Al-Ostaz A, Jasiuk I, Ostoja-Starzewski M (1998) Int J Solids Struct 35:2537
12. Chiaia B, Vervuurt A, Van Mier JGM (1997) Eng Fract Mech 57:301
13. Ostoja-Starzewski M (1998) Int J Solids Struct 35:2429
14. Ostoja-Starzewski M, Jasiuk I, Alzebdeh K, Al-Ostaz A (1996) In: Symposium on scaling laws for mechanics of fracture, 19th intl. congress of theoretical and applied mechanics, Kyoto, Japan
15. Ostoja-Starzewski M, Al-Ostaz A, Jasiuk I, Alzebdeh K (1996) In: Frangopol DM, Mircea D (eds) Probabilistic mechanics & structural reliability, Proceedings of the seventh specialty conference of ASCE, Grigoriu, p 362
16. Pyrz R (1994) Mater Sci Eng A177:253
17. Day A, Snyder K, Garboczi E, Thorpe M (1992) J Mech Phys Solids 40:1031
18. Ghosh S, Mukhopadhyay S (1993) Comput Methods Appl Mech Eng 104:211
19. Ghosh S, Lee K, Moorthy S (1996) Comput Methods Appl Mech Eng 132(1-2):63
20. Ghosh S, Lee KH, Moorthy S (1995) Int J Solids Struct 32 (1):27
21. Ghosh S, Mallett RL (1994) Comput Struct 50(1):33
22. Ghosh S, Mukhopadhyay SN (1991) Comput Struct 41(2):245
23. Ghosh S, Nowak Z, Lee K (1997) Compos Sci Technol 57:1187
24. Ghosh S, Nowak Z, Lee K (1997) Acta Mater 45(6):2215
25. Ghosh M, Moran B, Achenbach J (1994) Int J Damage Mech 3:357
26. Zhang J, Katsube N (1995) Finite Elements Anal Design 19:45
27. Gong SX, Meguid SA (1993) Acta Mech 99:49
28. Daniel IM, Durelli J (1962) Exp Mech 2:240
29. Marloff R, Denial I (1969) Exp Mech 9:156
30. Pijaudier-Cabot G, Bazant ZP (1992) J Eng Mech ASCE 11310):1512
31. Kachanov M (1987) Int J Fract 28:11
32. Alzebdeh KI (1994) PhD dissertation, Michigan State University
33. Pyrz R (1994) Comp Sci Tech 50:197
34. Pyrz R, Bochenek B (1994) Sci Eng Compos Mater 3(9):5
35. Pyrz R, Bochenek B (1995) IUTAM symposium on microstructure-property interactions in composite materials, p 313
36. Pyrz R, Bochenek B (1998) Int J Solids Struct 35:2413
37. Axelsen MS, Pyrz R (1997) IUTAM symposium on microstructure-property interactions in composite materials, p 15
38. http://www.aub.auc.dk/phd/department15/text/axelsen.pdf
39. Green PJ, Sibson R (1977) The Comput J 21(2):168
40. Gilbert EN (1962) Ann Math Statist 33:958
41. Anipindi D (2004) Master Thesis, University of Mississippi
42. Benjamin JR, Cornell CA (1989) Probability, statistics and decision for civil engineers. McGraw-Hill Publishing Company

43. James EG (1998) Random number generation and Monte Carlo Methods. Springer Publishers
44. O'Rourke J (1998) Computational geometry in C, 2nd edn. Cambridge University Press
45. Heath MT (2002) Scientific computing, an introductory survey, 2nd edn. McGraw-Hill Publishing Company, New York
46. Stauffer D, Aharany A (1992) Introduction to percolation theory, 2nd edn. Taylor and Francis Ltd, London
47. Takahashi J, Suito H (2001) Acta Mater 49(4):711
48. Pfeiffer PE (1995) Basic probability topics using Matlab. PWS Publishing Company
49. http://www.mathworld.wolfram.com/topics/StatisticalDistributions.html
50. http://www.ocw.mit.edu/NR/rdonlyres/Materials-Science-and-Engineering/3-11Mechanics-of-MaterialsFall1999/5991E176-AC60-4399-87F0-86AE35963750/0/composites.pdf
51. http://www.cse.uiuc.edu/heath/scicomp/notes/chap13.pdf
52. Shan Z, Gokhale AM (2004) Comput Mater Sci 24:361
53. Kanit T, Forest S, Galliet I, Mounoury V, Jeulin D (2003) Int J Solids Struct 40:3647
54. Stroeven M, Askes H, Sluys LJ (2004) Comput Methods Appl Mech Eng 193:3221
55. Swaminathan S, Ghosh S, Pagano NJ (2006) J Compos Mater 40:583
56. Swaminathan S Ghosh S, Pagano NJ (2006) J Compos Mater 40:605
57. Ostoja-Starzewski M (2006) Probabilist Eng Mech 21:112
58. ANSYS 7.0 User Manual. Swanson Analysis Systems, Inc., Houston (2002)
59. Hashin Z (1983) J Appl Mech 50:481
60. Hashin Z (1962) J Appl Mech 29:143
61. Mura T (1998) Micromechanics of defects in solids. Kluwer Academic Publishers, Dordrecht
62. Sulivian BJ, Hashin Z (1990) Controlled interfaces in composite materials. Elselvier, New York, p 521
63. Christensen RM (1991) Mechanics of composite materials. Krieger Publishing Company, Malabar Florida